Real-Time Ultrasound Imaging of a Human Muscle to Optimize Shared Control in a Hybrid Exoskeleton

Ashwin Iyer, Ziyue Sun, Krysten Lambeth , Mayank Singh , Christine Cleveland, and Nitin Sharma

Abstract—A hybrid exoskeleton is a class of wearable robotic technology that simultaneously uses a powered exoskeleton and functional electrical stimulation (FES) to generate assistive joint torques for people with impaired mobility due to neurological disorders such as spinal cord injury (SCI). The hybrid assistive technology benefits from FES that actively elicits force from paralyzed muscles via their neural excitation, leading to muscle strengthening. The main technical barrier to realizing the hybrid technology is to attain stable coordination between FES and the exoskeleton despite the quick onset of FES-induced muscle fatigue, which causes a rapid decline in the muscle force. Current methods to measure the induced fatigue lack direct muscle state measurements and may be ineffective at capturing the muscle force decay due to FES. Instead, ultrasound (US) imaging accurately quantifies FES-related muscle contractility and fatigue due to the direct visualization of muscle fibers. In this article, we use real-time US imaging-derived muscle strain changes as biomarkers of FES-induced fatigue in an optimal controller that modulates exoskeleton assistance and FES dosage. To demonstrate that real-time US imaging is a promising muscle–machine interface technology that can optimize shared control in a hybrid exoskeleton, we perform experiments involving continuous seated knee extension and over-ground walking tasks on two participants with SCI and four participants without disabilities. Furthermore, this work helps design a novel and unprecedented robotic gait technology with the capability to impart FES-associated therapeutic benefits while assisting the gait of neurologically impaired individuals, including those with SCI, stroke, multiple sclerosis, etc.

Index Terms—Biomedical imaging, electrical stimulation, exoskeletons, neurorehabilitation, optimal control.

Ashwin Iyer, Krysten Lambeth, and Nitin Sharma are with the Joint Department of Biomedical Engineering, North Carolina State University, Raleigh, NC 27606 USA, and also with the University of North Carolina, Chapel Hill, NC USA (e-mail: ashwin.iyer2@gmail.com; kflambet@ncsu.edu; nsharm23@ncsu.edu).

Ziyue Sun is with Didi Research America LLC., Mountain View, CA 94043 USA (e-mail: sunzowei@gmail.com).

Mayank Singh is with Electrical and Computer Engineering Department, North Carolina State University, Raleigh, NC 27606 USA (e-mail: msingh25@ncsu.edu).

Christine Cleveland is with the Department of Physical Medicine and Rehabilitation, The University of North Carolina-Chapel Hill, NC 27514 USA (e-mail: Christine_Cleveland@med.unc.edu).

This article has supplementary downloadable material available at https://doi.org/10.1109/TRO.2024.3443668, provided by the authors.

Digital Object Identifier 10.1109/TRO.2024.3443668

I. INTRODUCTION

PARAPLEGIA (paralysis) and paraparesis (weakness) are debilitating outcomes of spinal cord injury (SCI) that result in mobility limitations, such as difficulty transferring to standing and walking. In the United States alone, 40.6% of approximately 288 000 people living with SCI have paraplegia, and thousands of new cases of SCI occur each year [1]. These mobility impairments result in frequent hospitalizations and preventable complications such as urinary tract infections and pressure injuries of the skin, with average lifetime medical costs exceeding $1 million per individual [2], [3]. In contrast, the functional and therapeutic benefits associated with enabling gait mobility for those with incomplete SCI leads to fewer secondary medical complications and rehospitalizations [4], [5].

Functional electrical stimulation (FES) is an assistive technology that induces active but artificial muscle contractions that have the potential to generate the power required to perform standing and walking tasks and thus help people with SCI recover mobility [6], yet FES is not widely used for standing and walking following SCI [7]. Notably, due to its nonphysiological manner of muscle recruitment, FES is prone to induce a rapid onset of muscle fatigue that limits its effectiveness in long-term periodic and high-powered motions such as walking or sitting-to-standing. This is more problematic in persons with chronic SCI, where due to muscle atrophy, muscle fiber-type composition changes to fast-fatiguing muscle fiber types [8], [9]. As a result, the force output of the stimulated muscle drops by 50% shortly after stimulation onset (compared to 30% in nonparalyzed muscles) [10]. Commonly, an orthosis is applied to stabilize the limbs in lieu of FES [11], foregoing the benefits of activating the lower-limb muscles to improve the kinematics and kinetics of walking. The use of an orthosis instead of FES is largely due to the inability of current technology to address muscle fatigue or compensate for its effect while synergistically adapting walking motion [12].

Recently, powered exoskeletons have emerged as a technology that can restore lower limb mobility during functions such as sit-to-stand and walking [13]. Potentially, robotic exoskeleton devices, when augmented with FES, can enhance the rehabilitative attributes of powered exoskeletons by helping users achieve active muscle contractions while simultaneously receiving assistance from the exoskeleton. The cooperative torque assistance from FES also reduces the power requirement from the robotic exoskeleton and potentially leads to portable, longer-lasting solutions [14], [15], [16].

The addition of FES creates actuator redundancy, which remains one of the primary challenges in the design and control of a hybrid exoskeleton. The control problem is nontrivial mainly because the designed controller needs to dynamically determine a proper FES dosage and motor torque while maintaining a desired lower limb motion despite the onset of muscle fatigue. Indeed, control methods have been developed to achieve a hybrid exoskeleton, but they address the control problem in an ad hoc manner. For example, proportional-integral-derivative control of an exoskeleton [17], [18] has been combined with muscle torque estimation [17] and event-based FES triggering [18] to coordinate FES and a hybrid exoskeleton. In [19], a switched control framework was designed to switch between control modes that used motors only and motors and FES based on a muscle fatigue level from a mathematical model. These control approaches do not optimally distribute control between FES and the exoskeleton or resolve actuator redundancy based on the muscle fatigue state. In this context, optimal control or dynamic optimization is more suitable for cooperative control of a hybrid exoskeleton. Studies in [20] and [21] used a model predictive control (MPC) approach to regulate the knee joint and determined the optimal FES and motor torque dosage based on a dynamic model (e.g., musculoskeletal model of a user). A major benefit of this control design is that it ensures state and input constraints, such as limits of FES dosage, are met. While promising, these MPC approaches use estimates of fatigue onset based on a dynamic fatigue model [22]. The fatigue model depends on an accurate initial condition and person-specific parameters, which potentially leads to model inaccuracy without the availability of a direct fatigue measurement to update the model. A key to effective shared control in a hybrid exoskeleton is to directly measure the muscle' s fatigue state, update the fatigue model, and then use an optimal control framework, such as MPC, to optimize and automate the distribution of inputs to FES and exoskeleton. However, sensors that provide direct, noninvasive physiological state measurements of targeted skeletal muscles are lacking. Current efforts to measure muscle fatigue include force measurements from load cells or dynamometers [23] and surface electromyography (sEMG) [24], [25], [26]. While a decay in isometric force generation is directly related to muscle fatigue, it is difficult to measure the fatigue of individual muscles within a group such as the quadriceps. Further, it is difficult to estimate force generation in a dynamic setting, and most dynamometers are not portable for real-time exoskeleton control. While helpful, these measures do not provide direct metrics of muscle-related changes due to FES-elicited contractions. sEMG is suitable to measure fatigue at the neuromuscular level but has its has its own limitations such as sensitivity to electrode placement, cross talk between neighboring muscles [25], inability to measure signals from deep muscles [25], and signal interference from electrical stimulation [27]. The lack of direct measurements of muscle fatigue may limit the maximization of FES dosage during therapy by not effectively modulating the administered FES in response to the fatigue level of the stimulated muscle. Thus, we believe that there is a need for real-time direct muscle fatigue feedback to assist a hybrid exoskeleton controller' s decision-making regarding FES and motor torque input. Ideally, if user-specific

muscle fatigue during FES can be monitored, the motor torque can be adjusted as a fatigue compensation technique (i.e., as the user's muscle fatigues, the hybrid exoskeleton will rely more on the motors to provide assistance until the muscle recovers).

Recently, ultrasound (US) imaging has been used as a noninvasive sensing modality to directly assess changes in muscle contractility [28], which may be used as an index to monitor muscle functions [29], [30], [31], [32]. US imaging is advantageous for multiple reasons. First, it has a relatively wide field of view (FOV) and has the capability to collect 2-D information on a targeted muscle in vivo. In addition, unlike sEMG signals, US imaging is unaffected by interference from FES artifacts and neighboring muscle activity. Further, in [33], US imaging was shown to be a viable approach for detecting isometric muscle contractions, and in [34], [35], [36], US imaging was used as a method for motion prediction in the upper limb. Overall, US imaging is beneficial because it concurrently provides a direct visualization of the desired muscles and a variety of US-derived signals, such as muscle thickness, pennation angle, and fascicle length, that can be used to analyze muscle contractility both superficially and at greater muscle depths. Our recent studies [37], [38], [39] highlight the potential use of US in closed loop control of assistive devices. In [38], US echogenicity signals from ankle muscles were fused with EMG to estimate muscle activation levels for use in an assist-as-needed controller during treadmill walking tasks. Sheng et al. [37] demonstrated that the axial strain derived from US images is a promising indicator of contractility change in the human quadriceps muscles due to FES-induced fatigue. US images were captured during isometric muscle contractions generated by FES, and a strain tensor was computed based on estimates of tissue motion in the captured images. Sheng et al.[39] investigated in vivo continuous variation of muscle contractility at different stages over the time course of the stimulation protocol. The correlation between the degraded contractility and the varying force produced by a repeatedly stimulated muscle was derived and validated on human participants, showing that US imaging can be a novel noninvasive sensing tool to measure the internal muscle state. When combined with predictive mathematical models of FES-induced force and fatigue, this will significantly improve their fatigue prediction. However, the studies in [37] and [39] performed US imaging analysis offline, leaving much room to investigate the use of real-time US-derived fatigue measurements.

The main objective of this article is to evaluate a real-time US-based sensing technique that has the capability of measuring FES-induced fatigue via changes in muscle contractility and informing an MPC-based control allocation framework (see Fig. 1). We designed an experimental protocol to study the use of real-time fatigue measurements in an MPC framework to track a continuous knee joint angle during seated knee flexion/extension and walking tasks on participants with and without SCI, while addressing the need for real-time state measurements of fatigue by using a graphical processing unit (GPU)-based implementation of the US imaging-driven adaptive speckle tracking algorithm in [37]. Further, we compare the US-derived real-time fatigue measurements during FES-elicited muscle contractions with the fatigue measurements from a dynamometer to validate
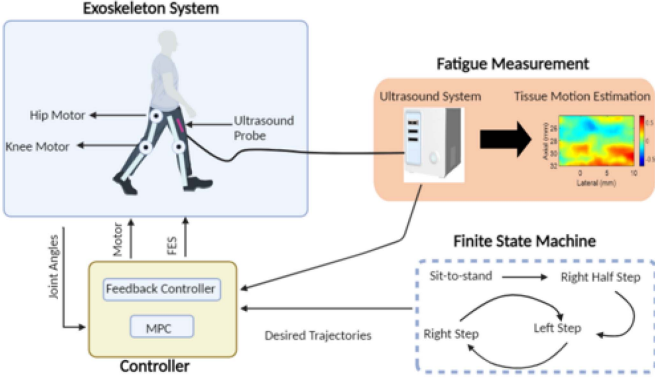
Fig. 1. Overview of proposed real-time US imaging technique for shared control. Measuring US-derived strain changes during isometric contractions in real-time could lead to more accurate allocation between FES and motors during shared control. As the muscle fatigues, the hybrid exoskeleton should reduce the FES input while increasing motor usage.

its real-time accuracy. We also compare the performance of the MPC scheme with real-time US-based measurements and with only the fatigue model to determine if inaccurate fatigue indication causes under/over-stimulation of the quadriceps. Because cooperative control between FES and exoskeleton may reduce the torque requirement from the exoskeleton, we also want to validate if the exoskeleton torques are reduced upon the addition of FES when compared to a case when only exoskeleton is used.

The innovation of this work lies in the use of real-time US-derived muscle strain signals that update a muscle fatigue and recovery model through quantifying muscle contractility changes. Particularly, we demonstrate the following contributions:

1) We develop and implement a real-time GPU-based architecture to measure muscle contractility from US images during FES-induced muscle contractions of the quadriceps.

2) We propose a sampled-data observer (SDO) structure to incorporate the real-time US measurement into a preexisting mathematical fatigue model.

3) The use of the SDO in an MPC framework is experimentally tested in both seated knee extension and walking tasks on two participants with SCI and four participants without disability.

The demonstrated work is significant to inform optimal control methods and fatigue characterization for US-based gait assistance. The research outcomes inform the design of a wearable exoskeleton gait technology that encourages using FES. The inclusion of FES can potentially infuse a variety of potential muscle health benefits (e.g., muscle strengthening, positive neuroplasticity, and cardiovascular fitness) while the elicited walking improves the quality of life and overall health goals post-SCI by increasing mobility and ambulation in social life. The rest of this article is organized as follows: Section II describes modeling of knee extension dynamics with US-derived fatigue measurements. The MPC development is shown in Section III. Section IV presents the real-time speckle tracking algorithm to estimate MEI. Section V shows the experimental study design.

Sections VI and VII present the results and discussion. Finally, Section VIII concludes this article.

II. KNEE EXTENSION DYNAMIC MODELING WITH REAL-TIME US DERIVED FATIGUE MEASUREMENTS

Our goal is to model and investigate cooperative control of a single degree of freedom leg extension model during both knee extension and walking tasks. The leg extension dynamics for a single degree of freedom musculoskeletal model are given as

$$J\ddot{\theta} + \tau_p(\theta, \dot{\theta}) + G(\theta) + w(t) = \tau \quad (1)$$

where $\theta, \dot{\theta}, \ddot{\theta} \in \mathbb{R}$ represent the angular position, velocity, and acceleration of the knee joint, $J \in \mathbb{R}^+$ is the moment of inertia of the leg, and $G(\theta) = mgl\sin(\theta + \theta_{eq})$ is a term that represents the torque due to gravity where $m \in \mathbb{R}^+$ is the mass of the lower leg, g is the gravitational acceleration constant, and $\theta_{eq} \in \mathbb{R}^+$ is the equilibrium position of the lower leg with respect to the vertical. $w(t) \in \mathbb{R}$ is an unknown disturbance, and τ_p is the passive torque of the knee joint and is modeled as $\tau_p(\theta, \dot{\theta}) = d_1(\phi - \phi_0) + d_2\dot{\phi} + d_3 e^{d_4\phi} - d_5 e^{d_6\phi}$, where $\phi, \dot{\phi}$ are the anatomical knee joint angle and angular velocity defined as $\phi = \frac{\pi}{2} - \theta - \theta_{eq}$, $\dot{\phi} = -\dot{\theta}$, and $d_i(i = 1, 2, \dots 6) \in \mathbb{R}$ are person-specific parameters. The total torque $\tau \in \mathbb{R}$ is the sum of torques generated from an electric motor and FES and is defined as $\tau = \tau_m + \tau_{ke}$, where τ_m is the motor torque and τ_{ke} is the torque generated by FES. The FES-elicited torque is modeled as

$$\tau_{ke} = \rho(\theta, \dot{\theta})\eta a \quad (2)$$

where

$$\rho(\theta, \dot{\theta}) = (c_2\phi^2 + c_1\phi + c_0)(1 + c_3\dot{\phi}) \quad (3)$$

is a positive, bounded function that represents nonlinear muscle length/muscle velocity dynamics, $c_i(0, 1, \dots, 3) \in \mathbb{R}$ are person-specific parameters, and $a \in [0, 1]$ is the muscle activation from FES. The activation is modeled as

$$\dot{a} = \frac{u_f - a}{T_a} \quad (4)$$

where $u_f \in [0, 1]$ is the normalized FES pulse width or current input, $T_a \in \mathbb{R}^+$ is a muscle activation time constant, and $\eta \in [\eta_{\min}, 1]$ is the FES-induced muscle fatigue, modeled as muscle effectiveness index (MEI)

$$\dot{\eta} = w_f(\eta_{\min} - \eta)a + w_r(1 - \eta)(1 - a) \quad (5)$$

where $w_f, w_r \in \mathbb{R}^+$ are fatigue and recovery time constants and $\eta_{\min} \in (0, 1)$ is the person-specific minimum MEI. Based on this model, when the muscle is rested, the MEI level is one, whereas when the muscle is completely fatigued, the MEI is $\eta_{\min}$.

A. Fused Real-Time US Imaging-Based MEI Estimate

Our goal is to update the model in (5) with normalized strain measurements from US images obtained at a lower sampling frequency than the exoskeleton controller. To achieve this, we use a SDO structure to fuse each independent US-derived strain

measurement with the model defined as

$$\dot{\hat{\eta}} = w_f(\eta_{\min} - \hat{\eta})a + w_r(1 - \hat{\eta})(1 - a) + \lambda\tilde{\eta}(t_k) \quad (6)$$

where $\hat{\eta}$ is the estimated MEI, a is the muscle activation from a normalized FES current input, $\lambda \in \mathbb{R}^+$ is a positive gain, and

$$\tilde{\eta}(t_k) = \hat{\eta}(t_k) - \eta(t_k) \quad (7)$$

where $\eta(t_k)$ is the normalized strain measurement obtained by US at time instant t_k and $\eta(t_k)$ is held constant until a subsequent measurement is available at t_{k+1}, with the time between two measurements denoted as T.

Theorem 1: The error between the model in (5) and the SDO in (6) asymptotically converges to zero if λ is chosen as $\frac{2w_r}{3} \leq \lambda \leq 2w_r$ and the sampling time between two consecutive US measurements is $\frac{2}{2w_r - \lambda}\ln(\frac{\lambda + 2w_r}{3\lambda - 2w_r}) > T$.

Proof: Choose a Lyapunov functional candidate as

$$V(t) = \frac{1}{2}\tilde{\eta}^2 \quad (8)$$

where $\tilde{\eta}$ is defined in (7). Taking the derivative of $V(t)$, using the definitions of $\dot{\hat{\eta}}$ and $\hat{\eta}$, and using the assumption that $T_r > T_f$ (i.e., the muscle fatigues faster than it recovers and $w_r < w_f$), gives

$$\dot{V} = -(w_f - w_r)a\tilde{\eta}^2 - w_r\tilde{\eta}^2 + \tilde{\eta}\lambda\tilde{\eta}(t_k). \quad (9)$$

Invoking the lower bound on a and applying Young's Inequality gives

$$\dot{V} \leq -(w_r - \frac{\lambda}{2})\tilde{\eta}^2 + \frac{1}{2}\lambda\tilde{\eta}^2(t_k). \quad (10)$$

Provided $\lambda < 2w_r$, $\dot{V}$ can be further bounded as

$$\dot{V} \leq -\Upsilon V + \lambda V(t_k) \quad (11)$$

where $\Upsilon = w_r - \frac{\lambda}{2}$. Multiplying both sides of (11) by $e^{\Upsilon t}$ and integrating on the interval $[t_k, t_{k+1}]$ gives

$$V(t_{k+1}) \leq \varsigma V(t_k) \quad (12)$$

where

$$\varsigma = \left[\frac{\lambda}{\Upsilon} - \frac{\lambda}{\Upsilon}e^{-\Upsilon T} - e^{-\Upsilon T}\right]. \quad (13)$$

For any iteration k, it can be seen that

$$V(t_k) \leq \varsigma^k V(t_0). \quad (14)$$

It is clear that if $\varsigma \leq 1$, $V(t_k)$ approaches zero as k increases.

To determine bounds on λ that satisfy $\varsigma \leq 1$, and noting that $\lambda \leq 2w_r$, define auxiliary variable $\bar{\delta}$ such that $\lambda = 2w_r - \bar{\delta}$. Rearranging the terms of $\varsigma \leq 1$ and substituting $\lambda = 2w_r - \bar{\delta}$ into (13) gives

$$\frac{4w_r - 2\bar{\delta}}{\bar{\delta}} - 1 \leq e^{-(\frac{\bar{\delta}}{2})T}\left(\frac{4w_r - 2\bar{\delta}}{\bar{\delta}} + 1\right). \quad (15)$$

Further algebraic manipulation yields

$$T \leq \frac{2}{\bar{\delta}}\ln\left(\frac{4w_r - \bar{\delta}}{4w_r - 3\bar{\delta}}\right). \quad (16)$$

Substituting λ back into (16) gives

$$T \leq \frac{2}{2w_r - \lambda}\ln\left(\frac{\lambda + 2w_r}{3\lambda - 2w_r}\right). \quad (17)$$

Thus, if $\frac{2w_r}{3} < \lambda \leq 2w_r$ is satisfied, and if the sampling time between consecutive US measurements satisfies (17), it is true that $\varsigma < 1$. Thus, from (14), the error between the augmented and nominal model in (7) converges to zero.

III. MPC FRAMEWORK

The goal of the MPC framework as previously shown in [40] is to determine the motor and FES inputs, τ_m and u_f, to track a desired joint angle trajectory $\theta_d(t) \in \mathbb{R}$. In this framework, parameters for the nominal leg extension model without any disturbances are denoted by $\bar{x}$, while x is a generalized state of the actual system. To achieve this goal, a tracking error term $e \in \mathbb{R}$ is defined as

$$e = \theta_d - \bar{\theta}. \quad (18)$$

To further ease the subsequent control development, we introduce an auxiliary error term $r \in \mathbb{R}$ that is defined as

$$r = \dot{e} + \alpha e \quad (19)$$

where $\alpha \in \mathbb{R}^+$ is a positive gain. Introducing the auxiliary error term helps in rewriting the second-order dynamics in terms of the first-order dynamics. Further, an additional activation error, $e_x \in \mathbb{R}$, is introduced to accommodate the cascaded activation dynamics in (4) as

$$e_x = \bar{a} - \bar{a}_d \quad (20)$$

where $\bar{a}_d$ is a desired activation dynamics defined as $\bar{a}_d = \hat{\eta}^{-1}(\bar{J}_\rho(\ddot{\theta}_d + \alpha\dot{e}) + \bar{L}_\rho)$, where $\bar{J}_\rho$, $\bar{L}_\rho$ are defined as $\bar{J}_\rho = \frac{\bar{J}}{\bar{\rho}}$ and $\bar{L}_\rho = \frac{\bar{\tau}_p + \bar{G}}{\bar{\rho}}$ for nominal torque–length and torque–velocity relation $\bar{\rho}$ in (3). It is important to note that the FES control input does not directly influence the knee dynamics in (1) but appears in the dynamics of activation variable, a in (4). Thus, introducing the error term, e_x, helps to design the FES control input, u_f.

Taking the time derivative of (19) and using (18) and (1), the closed loop error system becomes [40]

$$\bar{J}_\rho\dot{r} = -\hat{\eta}e_x - \frac{\bar{\tau}_m}{\rho}. \quad (21)$$

Further, taking the time derivative of e_x in (20) gives an error dynamics that facilitates the design of the FES control input, $\dot{e}_x = \frac{1}{T_a}u_f - \frac{1}{T_a}\bar{a} - \dot{\bar{a}}_d$. Now, if one designs the FES input, u_f, as $u_f = T_a(v + \dot{\bar{a}}_d + \frac{\bar{a}}{T_a} + \hat{\eta}r)$, where $v(t) \in \mathbb{R}$ is the unknown control input to be determined by the MPC, the feedback linearized error dynamics is written as

$$\dot{e}_x = \hat{\eta}r + v. \quad (22)$$

Above, we have transformed the dynamics in (1)–(4) into first-order dynamics. Further, by defining a nominal state $\bar{x} \in \mathbb{R}^3$ as $x = [e \quad r \quad e_x]^T$ and control input $\bar{u} \in \mathbb{R}^2$ as

$$\bar{u} = \begin{bmatrix} \bar{\tau}_m & v(t) \end{bmatrix}^T \quad (23)$$

the first-order error system in (19), (21), and (22) is written for MPC formulation as

$$\dot{\bar{x}} = \begin{bmatrix} r - \alpha e \\ \frac{1}{\bar{J}_\rho}[-\hat{\eta}e_x - \frac{\bar{\tau}_m}{\rho}] \\ \hat{\eta}r + \bar{u}_2 \end{bmatrix} = f(\bar{x}, \bar{u}). \tag{24}$$

The MPC framework determines the optimal $\bar{u}$ in (23) by solving the optimization problem

$$\min_{\bar{u}} \int_{t_k}^{t_k+T} l(\bar{x}, \bar{u})dt + V(\bar{x}(t_k + T)) \tag{25}$$

subject to

$$\dot{\bar{x}} = f(\bar{x}, \bar{u})$$
$$\dot{\hat{\eta}} = w_f(\eta_{min} - \hat{\eta})\bar{a} + w_r(1 - \hat{\eta})(1 - \hat{\eta}) + \lambda\tilde{\eta}(t_k)$$
$$\bar{x}(t_k + T) \in \Omega_T$$
$$\bar{u} \in U$$
$$T_a\dot{a}_d \le 1 - T_a\Omega_r - T_a\gamma_2 \tag{26}$$

where U is a set of control inputs that bounds $\bar{u}$ and Ω_T is a terminal region defined as

$$||\bar{x}(t_k + T)||^2 \le 3\frac{\gamma_1^2 + \gamma_2^2}{k_s^2 + k^2} \tag{27}$$

where $\gamma_1, \gamma_2, k_s, k \in \mathbb{R}^+$ are positive control gains.

The running cost $l(x, u)$ and terminal cost $V(x(t_k + T))$ in (25) are defined as

$$l(x, u) = \bar{x}^T Q\bar{x} + \bar{u}^T R\bar{u}$$
$$V(x(t_k + T)) = \frac{1}{2}e^2 + \frac{1}{2}\bar{J}_\rho r^2 + \frac{1}{2}e_x^2 \tag{28}$$

where $Q \in R^{3\times3}$ and $R^{2\times2}$ are positive definite, symmetric matrices. The terminal region and terminal cost are introduced to ensure recursive feasibility of the MPC framework [40].

To account for disturbances between the measured states and the states from the nominal model, a nonlinear feedback controller is designed as

$$u_{fd} = \vartheta(||\sigma||)||\sigma||\text{sat}\left(\frac{\delta}{\varepsilon_1}\right) + \varpi\text{sat}\left(\frac{\delta}{\epsilon_1}\right) + \kappa\delta \tag{29}$$

where $\varepsilon_1, \kappa \in \mathbb{R}^+$ are gains, ϖ is the upper bound of the disturbance to the nominal system $w(t)$, and $\epsilon, \delta \in \mathbb{R}$ are terms that represent the error between the nominal and actual knee joint angle and are defined as

$$\epsilon = \bar{\theta} - \theta$$
$$\delta = \dot{\epsilon} + \beta\epsilon$$

where $\beta \in \mathbb{R}^+$ is a positive constant, $\sigma = [\delta \quad \epsilon]^T$, and $\vartheta(||\sigma||) \in \mathbb{R}^+$ is a positive monotonic bounded function such that

$$\tau_p(\theta, \dot{\theta}) - \tau_p(\bar{\theta}, \dot{\bar{\theta}}) + G(\theta) - G(\bar{\theta})$$
$$+ \bar{\rho}(\bar{\theta}, \dot{\bar{\theta}})\bar{a}\hat{\eta} - \rho(\theta, \dot{\theta})a\hat{\eta} + \beta J\delta - \beta^2 J\epsilon$$
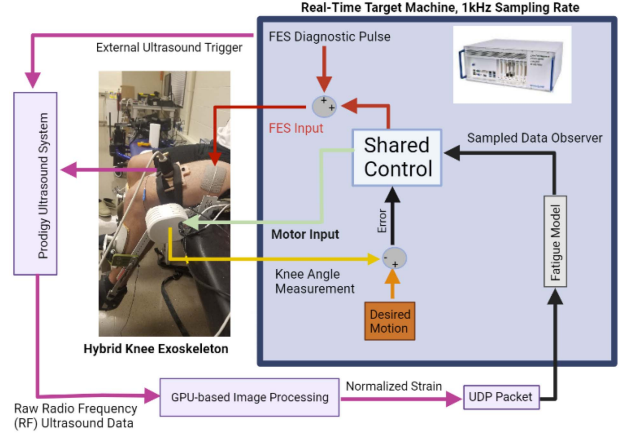$$\le \vartheta(||\sigma||)||\sigma||. \tag{30}$$

Fig. 2. Control framework of MPC with real-time US to perform knee extension tasks. A sinusoidal knee flexion-extension motion was performed for two minutes using MPC, which allocated FES and motors based on the US imaging-derived MEI. When the leg was in the vertical position during the trajectory, a diagnostic FES pulse was delivered to obtain an MEI estimate. As the muscle fatigues due to continuous stimulation from FES, the MPC should ensure that the FES dosage decreases and that the motor increases its contribution to guarantee joint angle tracking performance.

The total input that goes to the motor is then given as

$$\tau_m = \bar{\tau}_m + u_{fd}. \tag{31}$$

Equation[40] further derives a terminal controller to guarantee recursive feasibility and ensure that the control inputs of the original system stay within their constraints. The optimal control problem in (25) was solved in real-time using a fast gradient projection algorithm described in [41]. The overall implementation of the shared control framework during the knee extension study is shown in Fig. 2.

IV. REAL-TIME GPU-BASED SPECKLE TRACKING TO ESTIMATE MEI

In this section, we present a real-time US imaging based MEI estimation algorithm based on [37]. A speckle tracking algorithm was developed to measure tissue motion during FES-induced contractions. It was observed that as the quadriceps fatigued, the decay in tissue motion correlated with the force decay from FES-induced fatigue. The speckle tracking algorithm consists of the following steps:

1) Determine the tissue motion between two consecutive US images m and n by calculating a displacement matrix in axial (depth) and lateral directions at each spatial position (x, y) in the region of interest (ROI) of US images. The displacement matrix $d_{m,n}(x, y)$ is calculated as

$$d_{m,n}(x, y) = \underset{u,v}{arg\max}(\gamma(u, v)) \tag{32}$$

where $\gamma(x, y)$ is a normalized cross-correlation given as

$$\gamma(x, y) =$$
$$\frac{\sum_{K_{x,y}}(f_m(a, b) - \bar{f}_m)(f_n(a + u, b + v) - \bar{f}_{n,u,v})}{\sqrt{\sum_{K_{x,y}}(f_m(a, b) - \bar{f}_m)^2(f_n(a + u, b + v) - \bar{f}_{n,u,v})^2}} \tag{33}$$

where f_n, f_m are the magnitudes of the US image at spatial positions $a, b \in K_{x,y}$. $K_{x,y}$ is a rectangular kernel centered at (x, y), and u, v are displacement offsets that form a search window $K_{u,v}$ around (x, y). Further, $\bar{f}_m$ and $\bar{f}_n$ are averaged values of $f_m(a, b)$ and $f_n(a + u, b + v)$.

2) Spatially filter $d_{m,n}(x, y)$ to mitigate tracking noise between each pair of frames. A 21×11 pixel kernel was generated and centered around (x, y). The median value of $d_{m,n}(x, y)$ within the kernel was assigned to a filtered displacement map $d_f(x, y)$.

3) Accumulate the displacement with respect to the first image of the motion. The accumulated displacement at frame n, defined as $s_n(x, y)$, can be calculated as

$$s_n(x, y) = (x_n, y_n) - (x_0, y_0) \qquad (34)$$

where

$$(x_n, y_n) = (x_{n-1}, y_{n-1}) + d_{n-1,n}(x, y). \qquad (35)$$

4) Calculate axial strain by applying a Savitzky–Golay filter [42] on the cumulative displacement in the direction of propagation of US images.

It is noted that the computation time of the normalized cross-correlation increases quadratically with the size of the kernel, search window, and ROI. In addition, to estimate small tissue motion between a set of US images, it is necessary to interpolate the US images to obtain a smaller lateral resolution, thus increasing the number of spatial locations at which the correlation coefficient is computed. To overcome these challenges, because $\gamma(x, y)$ at each spatial location is independent, the speckle tracking algorithm was implemented using a parallel processing GPU framework in which each set of US images was loaded on a GPU, and all values of $\gamma(x, y)$ were computed simultaneously [43].

When using the GPU implementation, the fatigue estimate between two consecutive images is reduced from the time scale of minutes to < 1 s. To obtain a fatigue estimate for a full isometric contraction, the frame-to-frame displacement is accumulated across the total number of frames in the contraction. Thus, the total computation time is the time required to calculate tissue motion between two frames multiplied by the number of frames in the contraction. The final fatigue estimate is obtained by taking the gradient of the accumulated displacement in the direction of US propagation, and its computation time is dependent on the sizes of the kernel, search window, and ROI, the interpolation factor, and the contraction duration.

Since the fatigue measurement from US images is computed by accumulating displacement across multiple frames, the sampling frequency of US fatigue measurements is much lower than the control frequency of the exoskeleton. In addition, each measurement is treated as an independent sample, which indicates the strain during an independent contraction along with a noise component due to the tradeoff between robust speckle tracking parameters and computation time. The SDO addresses these issues by fusing the fatigue model with each measurement. The workflow for the GPU-adapted speckle tracking algorithm is shown in Fig. 3.

In our previous studies [37], [39], US images were captured during isometric contractions within a fatiguing protocol, and
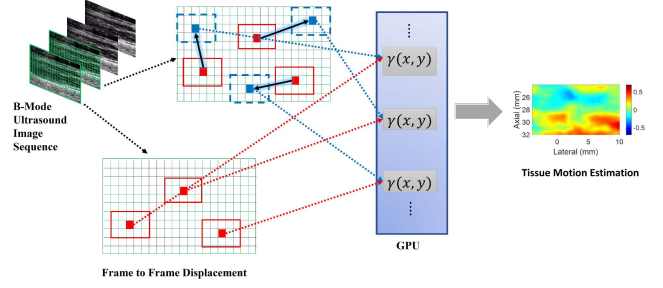

Fig. 3. Parallel computation of an adaptive speckle tracking algorithm to measure real-time strain changes. The displacements at each point in the region of interest (ROI, green squares) between two US images are independent and can be computed simultaneously. US images are loaded onto the GPU, and the tissue motion at each point is computed using in parallel NVIDIA' s CUDA architecture. The solid red squares highlight original tracking points with solid lines indicating the surrounding kernels in the original frame, while the blue squares represent the displaced points in the tracking frame. Red highlights a positive strain (i.e., tension), while blue represents a negative strain (i.e., compression) in the direction of propagation of US.

strain measurements were computed offline, providing the capability of analyzing larger ROIs and prolonged muscle contractions. To mimic these methods in a real-time exoskeleton control environment, we designed a diagnostic stimulation protocol for both knee extension and walking tasks. The diagnostic stimulation protocol consists of a one-second diagnostic pulse applied at a point during the desired trajectory at which the knee joint has zero velocity to ensure a quasi-isometric contraction. During the diagnostic pulse, the US system was delay triggered to collect raw radio frequency (RF) data and transfer it to the GPU platform (Titan V, NVIDIA, USA) after 150 ms of stimulation. The delayed trigger accounted for electromechanical delay when estimating the muscle response to FES. All images were reconstructed by sum and delay beamforming, and the US speckle tracking was implemented on the GPU. The MEI, $\eta(t_k)$ at time t_k in (7), is then calculated by averaging the strain at each pixel in the ROI and normalizing to the first contraction in the trial. The fatigue measurement was then sent to the MPC via a data transfer protocol (UDP). The procedure can be summarized in the following steps:

1) Start diagnostic stimulation.
2) Trigger US system after 150 ms of stimulation.
3) Collect 1 s of US images at 100 Hz (100 images in total)
4) Beamform images and perform speckle tracking of the image sequence.
5) Average strain map of the final image, normalize, and send to exoskeleton controller.

It is noted that in real-time, Steps 1–5 provide a visualization of a partial muscle contraction in comparison to the offline approach during which the whole muscle contraction can be imaged. To image a longer contraction, the number of frames in Step 3 can be increased, thus increasing the computation time of a fatigue measurement.

V. EXPERIMENTAL DESIGN

All experimental procedures performed in this study were approved by the Institutional Review Board (IRB) at the North

TABLE I
PARTICIPANT DEMOGRAPHICS

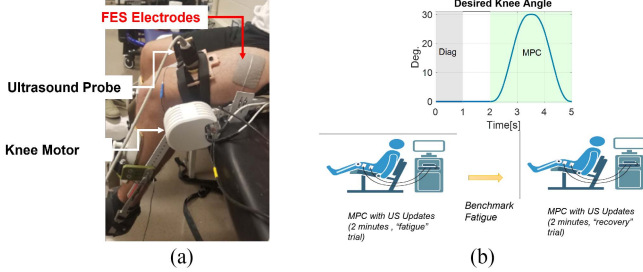| Participant	Age	Gender	Injury Level	Continuous Knee Extension (Leg)	Walking
B1	26	M	N/A	Yes (L,R)	No
B2	26	M	N/A	Yes (R)	Yes
B3	27	M	N/A	Yes (L,R)	Yes
B4	28	M	N/A	Yes (L)	No
S1	52	M	T10, incomplete	Yes (L,R)	Yes
S2	60	M	T7, complete	Yes (L,R)	Yes

Fig. 4. (a) Experimental setup for the continuous knee extension using a lab-developed exoskeleton. (b) MPC with real-time US was used to allocate FES and motors during a continuous knee extension task. Each participant performed two continuous knee extension trials during which the MPC framework tracked a sinusoidal trajectory for two minutes.

Carolina State University (IRB approval #: 20553). Four participants without disability and two participants with SCI were recruited to participate in this study. The overall study was broken into two sections: continuous knee extension and walking. During each section, the MPC framework to allocate FES and motors was implemented with and without US feedback. Details on each participant are shown in Table I.

A. Continuous Knee Extension

The framework and experimental setup for the continuous knee extension study is shown in Fig. 4. Participants were seated in a lab-fabricated exoskeleton as seen in Fig. 4(a) with the left knee joint actuated by an electric motor (Harmonic Drive LLC, MA, USA) and electrical stimulation of the quadriceps achieved using a commercial stimulator (Rehastim 2, HASOMED GmbH, Germany), which administered FES at a frequency of 33 Hz and a pulse width of 300 μ s through adhesive electrode pads (PALS, 7.62 cm by 10.16 cm, Axelgaard Manufacturing Co., Ltd., USA). A clinical US linear transducer (L7.5SC Prodigy Probe, S-Sharp, Taiwan) was placed longitudinally on the thigh and fixed by a customized probe holder to image the targeted quadriceps muscle.

Participants went through an experimental protocol that consists of two 2-min trials ("fatigue" and "recovery") during a seated knee extension task as shown in Fig. 4(b). The MPC with real-time US updates was administered to track a desired trajectory, shown in Fig. 4(b). Overall, each trial consisted of 24 knee extension repetitions resulting in a total of 96 knee extension repetitions throughout the whole study (fatigue trial, recovery trial, with and without US). The goal of the fatigue and recovery trial was to test allocation when the fatigue was initialized at different initial fatigue values. During the fatigue trial, because FES was being used for a 2-min duration, the

quadriceps would fatigue. The goal of the recovery trial is to determine allocation when the muscle starts at a fatigued state (i.e., during the recovery trial, the MPC should rely more on motors and less on FES, as compared to the fatigue trial, to maintain the tracking performance). During each trial, strain measurements were obtained for each knee extension cycle based on the diagnostic stimulation protocol and strain measurement algorithm described in Section IV. Thus, through the course of a single trial, 2400 images were processed overall.

Before and after each trial, participants sat in a dynamometer (Biodex, Medical Systems, NY, USA) and isometric torque measurements at the knee joint during a 1-s stimulation pulse were recorded as a benchmark for fatigue. In between the fatigue and recovery trial, real-time US measurements were collected based on a diagnostic pulse for comparison with the normalized isometric torque and model reinitialization.

B. Over-Ground Walking

The overall framework and experimental setup for the walking experiments is shown in Fig. 5. Two participants with no disability and two participants with SCI ($n = 4$) donned an INDEGO (Ohio, USA) exoskeleton embedded with FES capabilities as seen in Fig. 5(a) and performed four trials consisting of 20 steps (10 left, 10 right) in which the MPC framework was used to track the left knee trajectory during the gait cycle. Overall, each participant performed four trials of 20 steps with and without US resulting in a total of 80 steps taken in the exoskeleton. The linear transducer used in the walking experiments (L7.0SC Prodigy Probe, S-Sharp, Taiwan) was oriented and secured using medical tape as seen in Fig. 5(a) as to obtain transverse images of the quadriceps during the stance phase of each left step. This results in a total of 1000 US images collected during each walking trial.

At the beginning of each trial, real-time US measurements were collected to initialize the fatigue model for that trial. In addition, the participant started each trial in a seated position and performed a sit-to-stand task solely using a feedback controller before performing the walking. The trajectories for the sit-to-stand task were designed based on a virtual constraint method in [44].

The timing and control of the exoskeleton was governed by a finite state machine (FSM) with four states.
1) Sit-To-Stand.
2) Right Half Step.
3) Left Step.
4) Right Step.

The FSM started by transitioning from sit-to-stand followed by a right half step, and it proceeded to alternate between left step and right step for the entire 10 left step trial. The left and
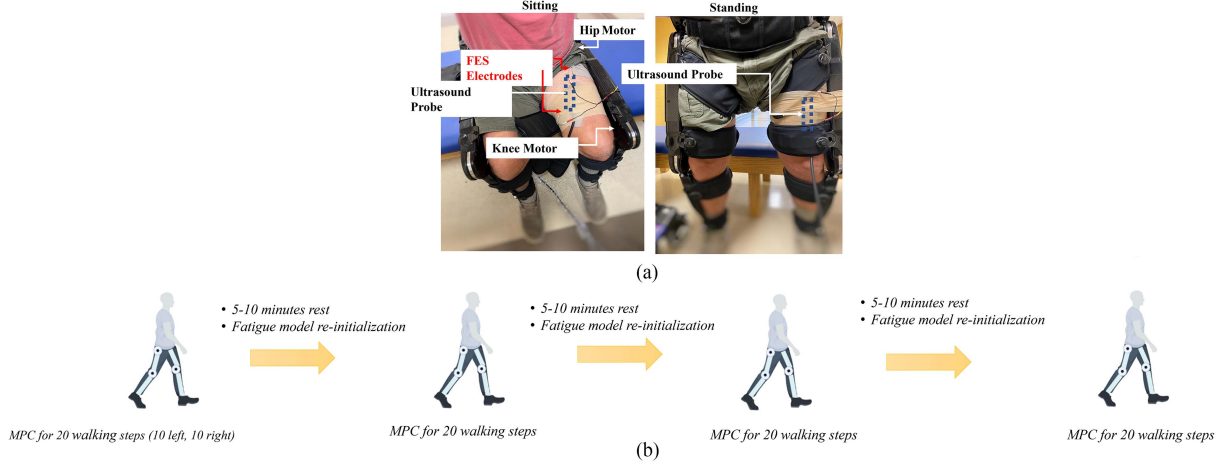
Fig. 5. (a) Experimental setup while a participant with SCI was seated and after they performed a sitting-to-standing task with assistance of the INDEGO exoskeleton, highlighting US probe placement during the walking trials. (b) Framework for experiments where MPC with real-time US is used to perform knee flexion/extension during a walking task. Each participant donned the exoskeleton and performed four trials of 20 steps (10 left, 10 right) during which the MPC was used to control knee flexion/extension on the left leg during the swing phase and a RISE controller was used on the right knee and both hip joints.
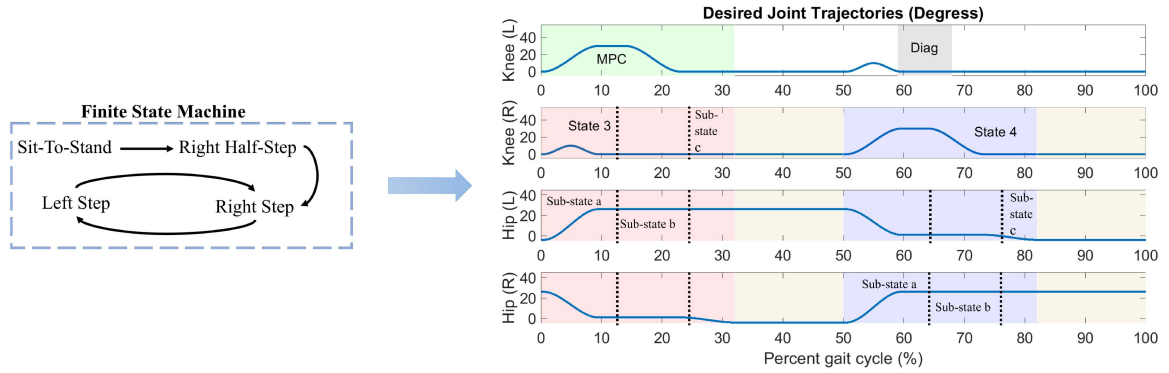

Fig. 6. Desired joint angle trajectories during states 3 (Left Step) and 4 (Right Step) of the FSM, highlighting the periods at which the MPC was utilized as well as the diagnostic pulse to collect US-driven MEI measurements.

right steps in states 3 and 4 were divided into the following three substates: a) swing leg hip and knee flexion, stance leg flexion/extension, b) swing leg knee extension, and c) stance leg hip extension.

The trajectory for each sub-state was designed using a third-order polynomial trajectory based on the desired angles of hip and knee flexion and extension. The desired flexion and extension angles for the hip and knee are highlighted in Fig. 5(b). The MPC algorithm was implemented on the left knee during knee flexion/extension of the swing phase, while the right knee and both hips were controlled by a robust-integral-signum-error (RISE) controller [45]. The RISE controller is given by the control law

$$\tau = k_1 e_2 + \int_0^t [k\alpha_2 + \beta\text{sgn}(e_2)]ds \qquad (36)$$

with tracking errors e_1, e_2 defined as

$$e_1 = \theta_d - \theta$$
$$e_2 = \dot{e}_1 + \alpha_1 e_1 \qquad (37)$$

where $k_1, \alpha_1, \alpha_2 \in \mathbb{R}^+$ are positive gains, $\theta_d(t) \in \mathbb{R}$ is the desired trajectory, $\theta(t) \in \mathbb{R}$ is the joint angle, and sgn is a signum function. Similar to the knee extension experiments, US imaging-based MEI measurements were received during each left step based on images collected during a diagnostic pulse to provide a quasi-isometric contraction, while the left leg was in the stance phase. The periods during which the quadriceps were stimulated by the MPC and by a diagnostic FES pulse are seen in Fig. 6.

VI. RESULTS

Experiments were performed on two participants with SCI and four participants without disability under two conditions: seated knee extension and over-ground walking. In each case, we compared the motor and FES inputs under conditions in which US was used as MEI feedback and when no US was used. We also compared the MEI from the model and from US images in the case in which US was used in the loop. To compare the MEIs from the Biodex dynamometer and from strain imaging, we normalized each modality for consistency with the MEI model.
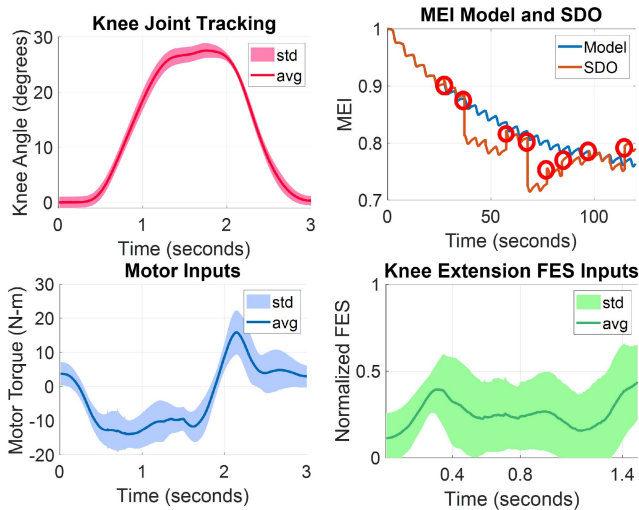
Fig. 7. Average joint angle, motor inputs, and knee extension FES inputs during the fatigue trial across all participants and all flexion/extension cycles along with representative MEI measurements (B3, right). Real-time US-derived measurements were used to update the model using a SDO approach at each time instant that US-based MEI measurements were available (indicated by the red circles).

A. Continuous Knee Extension Tracking and Actuator Allocation

The average root mean squared error (RMSE) between desired and actual trajectories for all participants was 2.74 ± 0.53 (mean $\pm$ STD) and 2.67 ± 0.41 degrees during the fatigue and recovery trials, respectively. The average knee joint position and motor and FES inputs along with the MEI profile with US updates for a participant without disability during the fatigue trial are shown in Fig. 7.

To determine a performance metric which highlights motor and FES usage, we computed the time integrals of motor torque and normalized FES for each knee extension cycle during the fatigue and recovery trials for all participants [see Fig. 8(a)]. The average integral of normalized FES during the fatigue and recovery trials was 0.38 ± 0.24 and 0.075 ± 0.056 s, respectively. The average integral of motor torque during the fatigue and recovery trials was 14.60 ± 4.26 and 20.96 ± 5.11 Nm-s, respectively. A one-tailed t-test revealed a significant difference in motor and FES inputs during the fatigue and recovery trial (one-tailed t-test, $p = 0.004$ for motors, $p = 0.009$ for FES, $\alpha = 0.05$).

The experimental protocol was repeated using only the MEI dynamic model in the MPC. In this case, the initial condition for the recovery trial was reinitialized from normalized isometric torque measurements. The average RMSE was 2.81 ± 0.60 and $2.78 \pm 0.61°$ during the fatigue and recovery trials, respectively, when the MPC allocation relied only on the MEI model without US-derived MEI updates. The RMSE for each trial and participant is shown in supplementary table S1. There is no significant difference in RMSE in either the fatigue or recovery trials when US is used as feedback compared to the fatigue model without US updates. The average integral of normalized FES during the fatigue and recovery trials with only the fatigue model was 0.43 ± 0.19 and 0.10 ± 0.07 s, respectively (one-tailed t-test, $p < 0.001, \alpha = 0.05$), while the average integral

of motor torque during the fatigue and recovery trials was 13.48 ± 2.86 and 18.21 ± 1.85 Nm-s, respectively (one-tailed t-test, $p = 0.001, \alpha = 0.05$). The integrals of normalized FES and motor torques for each participant with and without US feedback is shown in supplementary table S2.

B. Real-Time US Fatigue Measurements Compared to the Dynamic Model

We compared the MEI values during the final flexion/extension cycle of fatigue and recovery trials when US updates were used as feedback to using the model only. Due to the different fatigue rates of people with and without disability, we grouped their MEI values separately [see Fig. 8(b)]. For the participants with no disability, the average MEI after the final cycle of the fatigue trial with the model with US updates and with the model only was 0.69 ± 0.11 and 0.78 ± 0.05 (one-tailed t-test, $p = 0.046, \alpha = 0.05$), respectively. The average MEI value after the final cycle of the fatigue trial was 0.39 ± 0.01 and 0.46 ± 0.01 (one-tailed t-test, $p = 0.02, \alpha = 0.05$) for the participant with SCI. For the participants with no disability, the average final MEI value after the final cycle of the recovery trial with the model with US updates and with the model only was 0.55 ± 0.17 and 0.84 ± 0.03 (one-tailed t-test, $p = 0.004, \alpha = 0.05$), respectively. For the participant with SCI, the average MEI value after the final cycle of the recovery trial was 0.50 ± 0.02 and 0.90 ± 0.03 (one-tailed t-test, $p = 0.003, \alpha = 0.05$). The final MEI for each participant in each case is shown in supplementary table S3.

We further compared the integral of the total MEI over time across both fatigue and recovery trials with and without US updates [see Fig 8(c)]. For the participants with no disability, the average integral of MEI over both fatigue and recovery trials was 172.45 ± 17.43 and 201.48 ± 5.47 s with US updates and with the MEI model only, respectively (one-tailed t-test, $p = 0.004, \alpha = 0.05$). The average integral of MEI over both fatigue and recovery trials was 144.8 ± 3.39 and 167.90 ± 2.97 s for the participant with SCI when US updates and the MEI model only were used, respectively (one-tailed t-test, $p = 0.009, \alpha = 0.05$).

C. Benchmarking Real-Time US Measurements With MEI From a Dynamometer

It is seen in Fig. 7 that when a real-time US measurement is available, the SDO described in (6) is used to update the model. The amplitude of the difference in MEI between the model update and the original model is determined by the discrepancy between the model and measurement. However, it is unclear if the model or the measurement is closer to the true MEI of the muscle since the model is heavily dependent on system identification parameters and an accurate initial condition while the US measurement is susceptible to a variance and noise due to the discrete time points at which measurements are taken. To benchmark the US measurement, normalized strain values were collected after each trial as descried in the experimental procedure and compared to MEI recorded by the isometric torques [see Fig. 8(d)]. The average MEI from the US and the dynamometer after the fatigue trial was 0.76 ± 0.14 and 0.76 ± 0.13, respectively, and the average difference between
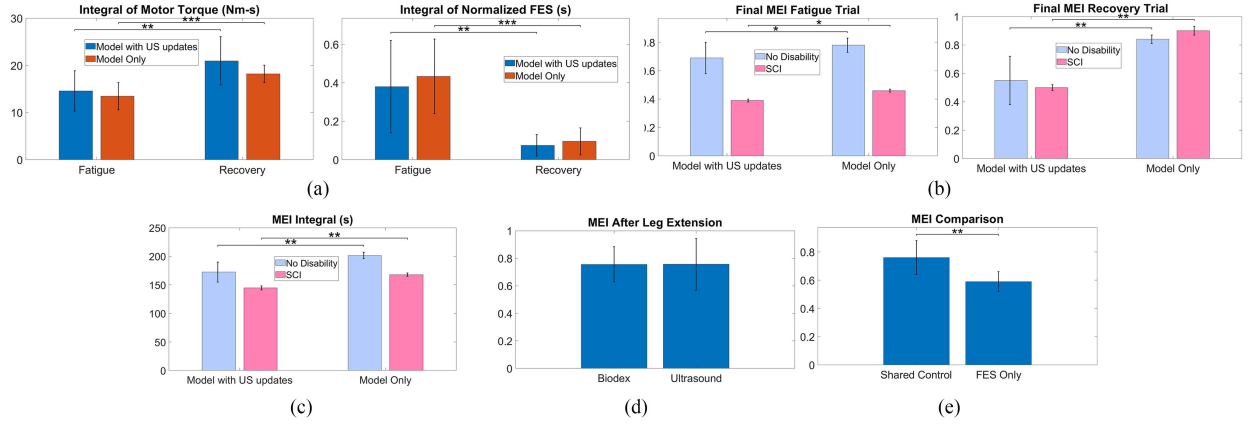
Fig. 8. Experimental results during a continuous knee extension task with MPC. (a) Integrals of average normalized FES and average motor torques across all knee extension cycles for all participants (with no disability and with SCI) during the fatigue and recovery trials. The integral of motor input increases during the recovery trial, while the FES integral decreases, indicating that as the muscle fatigues the hybrid exoskeleton uses less FES and more motor to perform the knee extension task. (b) Final MEI with and without US imaging-based feedback for the fatigue trial (left) and recovery trial (right) for both participant groups. (c) Integral of total MEI during the fatigue and recovery trials. The US measurements detect a lower MEI than just the fatigue model for both groups. (d) MEI based on decay in isometric torque during a diagnostic stimulation pulse measured from a dynamometer and from US imaging after continuous knee extension using MPC. The difference in MEI from US and isometric torque measurements is less than. 07 (7%) for all participants. (e) MEI from the dynamometer after the fatigue trial with real-time US measurements and shared control compared to fatigue measurements from the dynamometer when a feedback controller using only FES was used for continuous knee extension. The MPC with US measurements and shared control results in less fatigue.
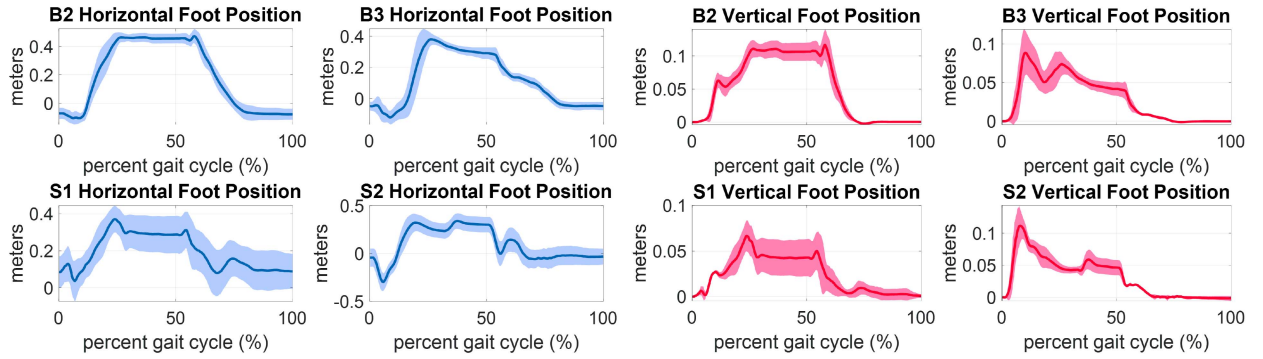

Fig. 9. Average horizontal and vertical foot placement of the left foot during the walking experiment during which the knee joint was controlled using MPC with US MEI updates with a shaded standard deviation for all participants. The foot position was calculated using forward kinematics from the left hip and knee joint angles. The labels B2 and B3 represent the kinematics from participants 2 and 3 from the group without disabilities, and S1 and S2 represent the two participants with SCI.

MEI measured from the dynamometer and real-time US was $0.03 \pm .02$. We performed a one-tailed t-test, which indicated no statistical difference between the MEIs from real-time US and the dynamometer ($p = 0.5, \alpha = 0.05$). This indicates that US-derived strain measurements can be used as an indicator of MEI in real time.

D. Comparison of Shared Control to FES Only Based Knee Extension

We conducted another isolated seated knee extension trial on all the participants with MPC to control only FES in which no US updates or motor was used in the controller. In this case, the average MEI measured from normalized isometric torque measurements was 0.59 ± 0.07. In comparison, the MPC for shared motor and FES assistance yielded the average MEI as 0.76 ± 0.12 (one-tailed t-test, $p = 0.01, \alpha = 0.05$) [see Fig. 8(e)].

E. Shared Control Framework With Real-Time US Measurements During Walking

To show the functionality of the walking framework, we computed the foot position of the left leg using forward kinematics. The average vertical and horizontal foot position of all 40 steps of the left leg controlled by the MPC with US measurements is shown in Fig. 9. A positive horizontal position represents the foot being in front of the hip, and a positive vertical position represents the foot being above the ground. The average RMSE in the horizontal direction between the desired and actual foot position across all four trials of 10 steps was 0.14 ± 0.006, 0.12 ± 0.01, 0.26 ± 0.006, and 0.17 ± 0.008 meters for the two participants with no disability and two participants with SCI, respectively. The average RMSE in the vertical direction was 0.03 ± 0.002, 0.03 ± 0.004, 0.09 ± 0.01, and 0.06 ± 0.004 meters for all participants, respectively. The RMSE for each
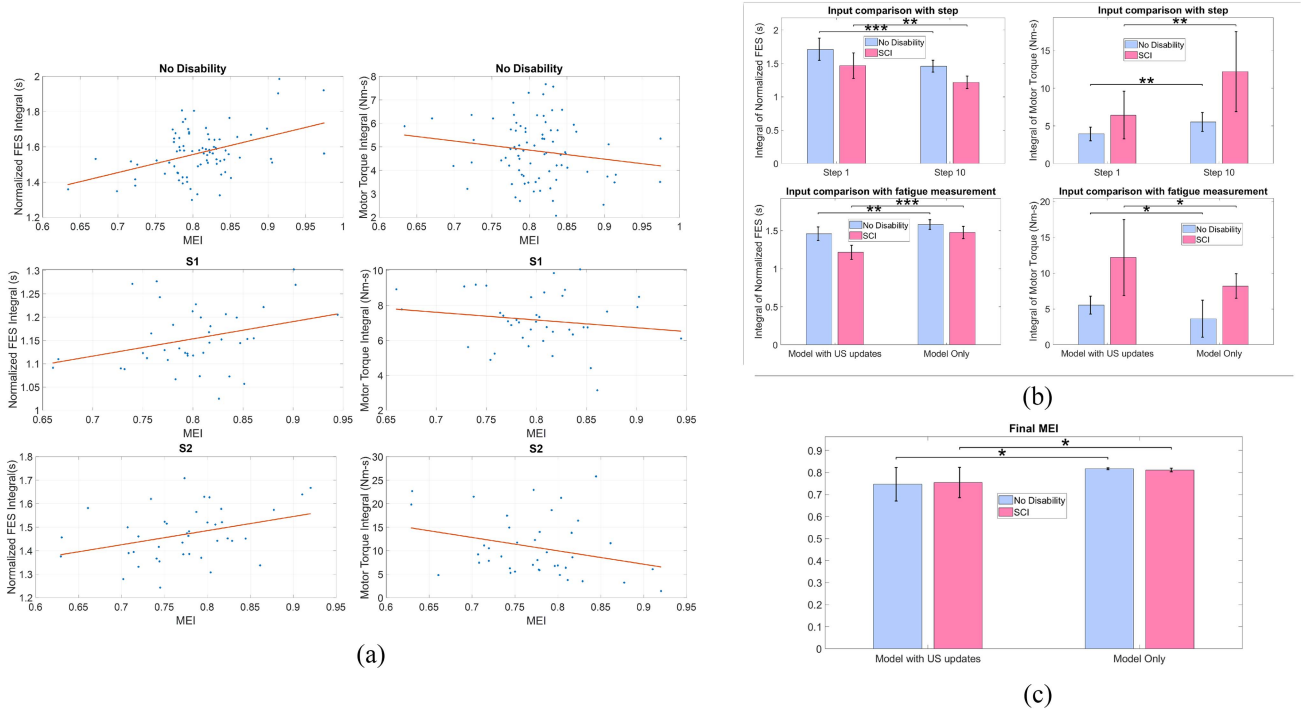
Fig. 10. Experimental results for the walking study performed on the INDEGO exoskeleton. (a) Integrals of FES and motor torque for each step plotted against the MEI measured from US images for participants with no disability (aggregated) and SCI along with a linear regression trend line. As MEI increases, the total integral of FES decreases, while the integral of motor torques increases.The labels S1 and S2 represent the two participants with SCI. (b) Integrals of FES and motor inputs during the 1st and 10th steps of each trial and integrals of FES and motor inputs after the 10th step of each trial with and without US feedback. (c) MEI during the 10th step of each trial for participants with and without disability when walking with MPC which uses the MEI model with US updates and the model only.

TABLE II
AVERAGE INTEGRALS OF MOTOR TORQUE AND NORMALIZED FES DURING THE SWING PHASE WHILE USING SHARED CONTROL WITH REAL-TIME US MEI UPDATES

Participant Category		Step 1	Step 10	p-value
SCI	FES (s)	1.47 ± 0.19	1.22 ± 0.09	0.004
	Motors (Nm-s)	6.44 ± 3.16	12.20 ± 5.32	0.002
No Disability	FES (s)	1.71 ± 0.17	1.46 ± 0.09	0.001
	Motor (Nm-s)	3.94 ± 0.91	5.53 ± 1.25	0.006

participant during each trial in the vertical and horizontal positions is shown in Table S4. To highlight the fatigue-based allocation during the walking task, we plotted the integral of FES and motor inputs for each step across all 40 steps against the MEI of each step derived from real-time US measurements along with a linear regression trend line [see Fig. 10(a)]. The results show that as the MEI decreases (i.e., more fatigue), the integral of normalized FES decreases while the integral of motor torques increases.

We additionally compared the integral of normalized FES during the swing phase of the 1st step of each trial with the integral of normalized FES during the swing phase of the 10th step [see Fig. 10(b)] as well as the integral of motor torque during the swing phase of the 1st and 10th steps for participants with and without disability. The average integrals of normalized FES and motor torques during the swing phase of the 1st and 10th steps for participants with and without disability are shown in Table II.

The individual integrals of normalized FES inputs and motor torques with and without US feedback during the 1st and 10th steps for all participants is shown in supplementary Tables S5–S8.

The experimental protocol was repeated on all four participants with the MPC relying on only fatigue dynamics instead of US feedback. The MEI for all participants at each step with US updates compared to the model only are shown in supplementary Fig. S1 and supplementary table S9. We compared the final MEI during the 10th step of each trial when US was used to update the model and when only the model was used in the MPC framework [see Fig. 10(c)]. The average MEIs during the 10th step are shown in Table III.We also compared the integral of normalized FES and motor torque during the swing phase of the 10th step with and without US feedback [see Fig. 10(b)]. The average integrals of normalized FES and motor torques during the swing phase of the 10th step with and without US updates are shown in Table IV.

TABLE III
AVERAGE MEI DURING THE 10TH STEP WHEN USING SHARED CONTROL WITH AND WITHOUT US UPDATES

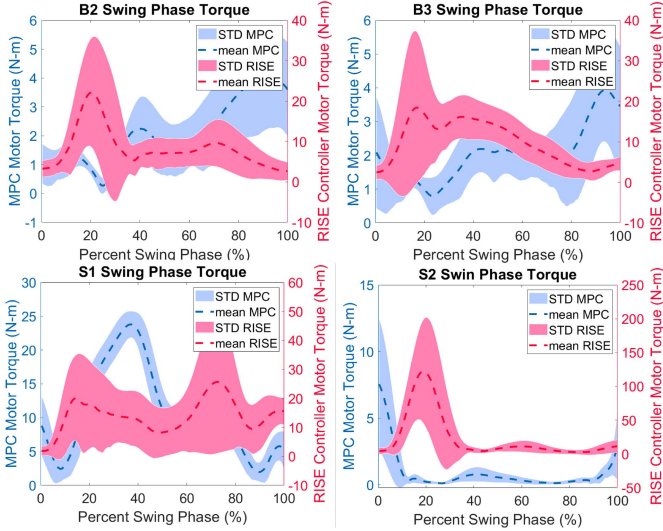| Participant Category	Model Only	Model with US update	p-value
SCI	0.81 ± 0.008	0.75 ± 0.07	0.02
No Disability	0.82 ± 0.004	0.75 ± 0.07	0.02

Fig. 11.   Mean and standard deviation of knee motor torques when using the RISE controller and MPC during the swing phase to perform a walking task.
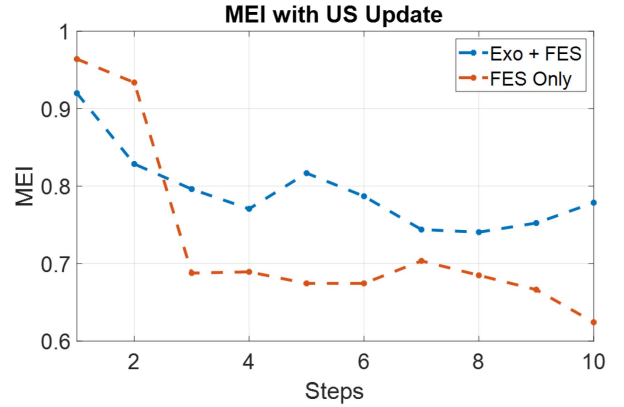

Fig. 12.   MEI at each walking step during the first walking trial based on fused US-model MEI measurements for both the shared control and FES only framework.

Finally, to verify the reduced power consumption of motors when using shared control, we compared the knee motor torques from the RISE controller on the right knee to the motor torques computed from the MPC as seen in Fig 11. The average integral of motor torque across the swing phase with the RISE controller and with MPC was 34.71 ± 16.88 and 9.83 ± 11.62 Nm-s, respectively (one-tailed t-test, $p = 0.03$, $\alpha = 0.05$).

F. Comparison of Shared Control With FES Only Walking

We additionally compared the shared control MPC framework with US measurements to an FES-only walking framework in which there was no motor assistance at the left knee joint. Participant S2 (injury level T-10) participated in two trials of 20 steps (10 left, 10 right). The fused MEI measurements between US and the fatigue model during the first trial for both FES only and the shared control framework are shown in Fig. 12. The integrals of MEI across the walking duration of two trials are 67.26 ± 2.96 and 77.32 ± 2.86 s when using FES only and shared control, respectively. This indicates that US-derived MEI is higher (less fatigue) in the case of shared control when compared to FES only for one participant with SCI, highlighting that using an exoskeleton along with FES can induce less fatigue due to lower FES dosage. This will likely improve fatigue resistance over an extended time compared to the FES-only case.

VII. DISCUSSION

We demonstrate using US imaging-derived strain measures in real-time with MPC to allocate inputs between FES and motors at the knee joint in a hybrid exoskeleton for both a continuous knee extension task and a walking task. The results of this study show that real-time US can be used as a biomarker for fatigue measurements in closed loop MPC algorithms. Specifically, real-time fatigue measurements from US imaging and a dynamometer differed by less than 7% for all participants [see Fig. 8(d)].

FES-induced fatigue leads to a sharp decay in force generation by the stimulated muscle, which can also be observed as a reduction in kinematic joint angle when performing dynamic tasks such as continuous knee extension and walking. In the presence of closed-loop control, the goal of which is to track a prescribed trajectory, the kinematic angle decay is not observable. In addition, since current state-of-the-art fatigue indicators such as dynamometers, load cells and sEMG are either difficult to incorporate into exoskeleton design, suffer from stimulation artifact interference, or do not directly indicate muscle fatigue state, there is a need for an alternative fatigue indicator. Based on the results from this study, direct fatigue measurement can be accomplished using US imaging.

The incorporation of US into the MPC algorithm was accomplished via a SDO to account for 1) the low sampling rate of US-based fatigue measurements due to memory limitations on the GPU as well as a tradeoff between measurement accuracy and speed and 2) mismatches between the fatigue differential model and real-time measurements. It is noted that the propagation of fatigue dynamics is highly dependent on fatigue and recovery time constants and a known initial condition. At the beginning of any periodic long-term FES task, it is assumed that the fatigue initial condition is one (no fatigue) since the muscle starts at a rested state, but any mismatch in time constants or initial condition will cause a discrepancy in the fatigue model. In contrast, the US-derived fatigue measurement detects unmodeled residual fatigue levels based on tissue motion. The SDO generates a continuous fatigue estimate that reinitializes whenever a fatigue measurement becomes available.

The MPC algorithm with real-time US measurements was also effective at performing knee flexion and extension during a walking task while allocating motor and FES. As seen in

Participant Category		Model Only	Model with US update	p-value
SCI	FES (s)	1.48 ± 0.08	1.22 ± 0.09	< 0.001
	Motors (Nm-s)	8.21 ± 1.72	12.20 ± 5.32	0.038
No Disability	FES (s)	1.58 ± 0.06	1.46 ± 0.09	0.03
	Motor (Nm-s)	3.64 ± 2.60	5.53 ± 1.25	0.047

Fig. 10(a), as the MEI increases, the integral of FES input during the swing phase trends negatively (i.e., as the muscle fatigues, less FES is used, and the motor torque contributes more effort) similar to Fig. 8(a), where the integral of motor inputs increases while the integral of normalized FES decreases during the recovery trial of the continuous knee extension experiments. This is further highlighted by the decrease in FES inputs between the 1st and 10th steps of each trial [see Fig. 10(b)]. Thus, the MPC with real-time US can adapt FES inputs based on fatigue level during a walking task.

In addition, from the comparison of the MEI at the 10th step for all participants when using MPC with US feedback to MEI at the 10th step when the MPC relied only on the model, it is seen that the final MEI from the US is lower (more fatigued) than when relying on the model [see Fig 10(c)]. This is consistent with the continuous knee extension study [see Fig. 8(b)]. Further, Fig. 10(b) shows the integral of FES during the 10th step for all trials when the MPC relies on US compared to only the model, and it is seen that the MPC with US feedback uses less FES than the MPC with only the model. Thus, the MPC scheme is more sensitive to fatigue when US updates are included than when relying only on the model. Simultaneously, it reduces the FES dosage and maintains good tracking performance of the knee joint. Thus, including real-time US in the MPC framework will lead to less overstimulation and could enable muscle recovery over extended periods of use. In addition to the therapeutic benefit of FES, another benefit when using MPC during walking is that the knee motors require less power than a traditional feedback controller, as seen in Fig. 11. The lower power requirement has implications in exoskeleton hardware design and has the potential to enable the use of more lightweight motors.

While the MPC with real-time US was shown to be effective at performing a walking task and the results indicate that the FES dosage and motor torque are allocated based on the MEI, it is seen that there are certain outliers in Fig. 10(a). This is because the goal of the MPC algorithm is to track a desired knee joint trajectory based on a leg extension model in (1), which does not account for forces such as ground reaction forces, which may be present during walking but not seated leg extension. Additional challenges arise with participants with SCI, such as limitations of the range of motion and the weakened strength of non-stimulated muscles such as hamstrings, ankle dorsiflexors, and plantar flexors. Further, desired trajectories from the FSM were designed individually as time-based third-order polynomial trajectories, leaving the possibility for coordination mismatch. One potential solution would be to consider a holistic walking model which includes trunk, hip, and knee dynamics as well as the ground

reaction forces and to design the trajectories based on virtual constraints.

The presented results show promise in using real-time US imaging as a fatigue biomarker in a hybrid exoskeleton. However, there are further limitations that should be addressed for full-scale implementation as a clinical rehabilitation technique. First, there is a tradeoff between real-time US computation time and measurement accuracy. The computation time using the GPU can be increased by reducing the size of the ROI of the quadriceps, size of the search window, kernel size, and duration of the FES-induced diagnostic contraction. Decreasing each of these parameters has the potential to lead to additional noise in the real-time US measurement, which could be corrected by parameters of the SDO. An alternative option is to tune the size of the ROI, kernel, size of the search window, and median filter parameters to track more precise displacements. This usually involves increasing the size of the ROI to track a larger region of the muscle as well as the size of the kernel and search window and would increase the sampling time, causing the MPC scheme to rely on fatigue from the model for a longer duration. Further, the computation time of US images can influence potential walking speeds of the exoskeleton. For the presented results, the trajectories were designed such that an MEI measurement was available at each left step. To increase walking speed while still receiving US updates, we could 1) relax speckle tracking parameters to speed up US image computation and/or 2) design the real-time US framework to obtain MEI measurements every Nth step, where $N = 2, 3, 4. \ldots$. The first option reduces the accuracy of each individual measurement, while option 2 increases the duration during which the MPC relies on the model without a US update and thus leaves room for overstimulation. Another challenge and potential problem for future research is developing a US imaging system that is easy to don and doff and that is more portable compared to the current US platform, which requires a GPU, monitor, and desktop setup. In our current experimental protocol, during the walking experiments, the US platform was wheeled with the participant as they walked in the exoskeleton, which creates a challenge of ensuring the probe does not slip from the quadriceps during each step. Developing a wearable US system that can detect real-time fatigue is the potential next step in clinical implementation.

VIII. CONCLUSION

Overall, this study established a real-time US fatigue algorithm, which can be used in conjunction with an MPC algorithm to allocate FES and motors in a hybrid exoskeleton based on the user's muscle fatigue level. The real-time fatigue measurements

were benchmarked with isometric torque measurements from a dynamometer and implemented in real-time to perform continuous leg extension as well as a walking task on a commercial exoskeleton. The implications of this study can be expanded to perform other functional rehabilitation tasks besides walking to improve the overall quality of life of people with SCI.

ACKNOWLEDGMENT

REFERENCES

[1] "Document citation: National spinal cord injury statistical center, traumatic spinal cord injury facts and figures at a glance," University of Alabama at Birmingham, Birmingham, AL, England, 2024.

[2] C. L. Gooch, E. Pracht, and A. R. Borenstein, "The burden of neurological disease in the United States: A summary report and call to action," *Ann. Neurol.*, vol. 81, no. 4, pp. 479–484, 2017.

[3] D. D. French, R. R. Campbell, S. Sabharwal, A. L. Nelson, P. A. Palacios, and D. Gavin-Dreschnack, "Health care costs for patients with chronic spinal cord injury in the veterans health administration," *J. Spinal Cord Med.*, vol. 30, no. 5, pp. 477–481, 2007.

[4] A. S. Gorgey, R. Wade, R. Sumrell, L. Villadelgado, R. E. Khalil, and T. Lavis, "Exoskeleton training may improve level of physical activity after spinal cord injury: A case series," *Top. Spinal Cord Inj. Rehabil.*, vol. 23, no. 3, pp. 245–255, 2017.

[5] S. A. Morrison, D. Lorenz, C. P. Eskay, G. F. Forrest, and D. M. Basso, "Longitudinal recovery and reduced costs after 120 sessions of locomotor training for motor incomplete spinal cord injury," *Arch. Phys. Med. Rehabil.*, vol. 99, no. 3, pp. 555–562, 2018.

[6] C. L. Lynch and M. R. Popovic, "Functional electrical stimulation," *IEEE Control Syst. Mag.*, vol. 28, no. 2, pp. 40–50, Apr. 2008.

[7] I. Bersch, S. Tesini, U. Bersch, and A. Frotzler, "Functional electrical stimulation in spinal cord injury: Clinical evidence versus daily practice," *Artif. Organs*, vol. 39, no. 10, pp. 849–854, 2015.

[8] J. L. Andersen, T. Mohr, F. Biering-Sørensen, H. Galbo, and M. Kjaer, "Myosin heavy chain isoform transformation in single fibres from m. vastus lateralis in spinal cord injured individuals: Effects of long-term functional electrical stimulation (FES)," *Pflügers Archiv*, vol. 431, pp. 513–518, 1996.

[9] R. K. Shields and S. Dudley-Javoroski, "Musculoskeletal plasticity after acute spinal cord injury: Effects of long-term neuromuscular electrical stimulation training," *J. Neuriophysiol.*, vol. 95, no. 4, pp. 2380–2390, 2006.

[10] R. J. Downey, M. J. Bellman, H. Kawai, C. M. Gregory, and W. E. Dixon, "Comparing the induced muscle fatigue between asynchronous and synchronous electrical stimulation in able-bodied and spinal cord injured populations," *IEEE Trans. Neural Syst. Rehabil. Eng.*, vol. 23, no. 6, pp. 964–972, Nov. 2015.

[11] S. Prenton et al., "Functional electrical stimulation versus ankle foot orthoses for foot-drop: A meta-analysis of orthotic effects," *J. Rehabil. Med.*, vol. 48, no. 8, pp. 646–656, 2016.

[12] G. M. Lyons, T. Sinkjær, J. H. Burridge, and D. J. Wilcox, "A review of portable FES-based neural orthoses for the correction of drop foot," *IEEE Trans. Neural Syst. Rehabil. Eng.*, vol. 10, no. 4, pp. 260–279, Dec. 2002.

[13] L. E. Miller, A. K. Zimmermann, and W. G. Herbert, "Clinical effectiveness and safety of powered exoskeleton-assisted walking in patients with spinal cord injury: Systematic review with meta-analysis," *Med. Devices: Evidence Res.*, pp. 455–466, 2016.

[14] A. J. Del-Ama, Á. Gil-Agudo, J. L. Pons, and J. C. Moreno, "Hybrid FES-robot cooperative control of ambulatory gait rehabilitation exoskeleton," *J. Neuroeng. Rehabil.*, vol. 11, no. 1, pp. 1–15, 2014.

[15] A. J. Del-Ama, A. D. Koutsou, J. C. Moreno, A. De-Los-Reyes, Á. Gil-Agudo, and J. L. Pons, "Review of hybrid exoskeletons to restore gait following spinal cord injury," *J. Rehabil. Res. Develop.*, vol. 49, no. 4, pp. 497–514, 2012.

[16] K. H. Ha, H. A. Quintero, R. J. Farris, and M. Goldfarb, "Enhancing stance phase propulsion during level walking by combining FES with a powered exoskeleton for persons with paraplegia," in *Proc. IEEE Annu. Int. Conf. IEEE Eng. Med. Biol. Soc.*, 2012, pp. 344–347.

[17] K. H. Ha, S. A. Murray, and M. Goldfarb, "An approach for the cooperative control of FES with a powered exoskeleton during level walking for persons with paraplegia," *IEEE Trans. Neural Syst. Rehabil. Eng.*, vol. 24, no. 4, pp. 455–466, Apr. 2016.

[18] M. A. Alouane, W. Huo, H. Rifai, Y. Amirat, and S. Mohammed, "Hybrid FES-exoskeleton controller to assist sit-to-stand movement," *IFAC-PapersOnLine*, vol. 51, no. 34, pp. 296–301, 2019.

[19] Z. Sheng, Z. Sun, V. Molazadeh, and N. Sharma, "Switched control of an n-degree-of-freedom input delayed wearable robotic system," *Automatica*, vol. 125, 2021, Art. no. 109455.

[20] N. A. Kirsch, X. Bao, N. A. Alibeji, B. E. Dicianno, and N. Sharma, "Model-based dynamic control allocation in a hybrid neuroprosthesis," *IEEE Trans. Neural Syst. Rehabil. Eng.*, vol. 26, no. 1, pp. 224–232, Jan. 2018.

[21] X. Bao, Z. Sheng, B. E. Dicianno, and N. Sharma, "A tube-based model predictive control method to regulate a knee joint with functional electrical stimulation and electric motor assist," *IEEE Trans. Control Syst. Technol.*, vol. 29, no. 5, pp. 2180–2191, Sep. 2021.

[22] R. Riener, J. Quintern, and G. Schmidt, "Biomechanical model of the human knee evaluated by neuromuscular stimulation," *J. Biomech.*, vol. 29, no. 9, pp. 1157–1167, 1996.

[23] N. K. Vøllestad, "Measurement of human muscle fatigue," *J. Neurosci. Methods*, vol. 74, no. 2, pp. 219–227, 1997.

[24] D. R. Rogers and D. T. MacIsaac, "EMG-based muscle fatigue assessment during dynamic contractions using principal component analysis," *J. Electromyogr. Kinesiol.*, vol. 21, no. 5, pp. 811–818, 2011.

[25] M. Cifrek, V. Medved, S. Tonković, and S. Ostojić, "Surface EMG based muscle fatigue evaluation in biomechanics," *Clin. Biomech.*, vol. 24, no. 4, pp. 327–340, 2009.

[26] A. Georgakis, L. K. Stergioulas, and G. Giakas, "Fatigue analysis of the surface EMG signal in isometric constant force contractions using the averaged instantaneous frequency," *IEEE Trans. Biomed. Eng.*, vol. 50, no. 2, pp. 262–265, Feb. 2003.

[27] F. Mandrile, D. Farina, M. Pozzo, and R. Merletti, "Stimulation artifact in surface EMG signal: Effect of the stimulation waveform, detection system, and current amplitude using hybrid stimulation technique," *IEEE Trans. Neural Syst. Rehabil. Eng.*, vol. 11, no. 4, pp. 407–415, Dec. 2003.

[28] R. S. Witte, K. Kim, B. J. Martin, and M. O'Donnell, "Effect of fatigue on muscle elasticity in the human forearm using ultrasound strain imaging," in *Proc. Int. Conf. IEEE Eng. Med. Biol. Soc.*, 2006, pp. 4490–4493.

[29] K. Bouillard, A. Nordez, and F. Hug, "Estimation of individual muscle force using elastography," *PLoS One*, vol. 6, no. 12, 2011, Art. no. e29261.

[30] P. Andonian et al., "Shear-wave elastography assessments of quadriceps stiffness changes prior to, during and after prolonged exercise: A longitudinal study during an extreme mountain ultra-marathon," *PLoS One*, vol. 11, no. 8, 2016, Art. no. e0161855.

[31] J. A. Hides, C. A. Richardson, and G. A. Jull, "Use of real-time ultrasound imaging for feedback in rehabilitation," *Manual Ther.*, vol. 3, no. 3, pp. 125–131, 1998.

[32] J. Heckmatt, N. Pier, and V. Dubowitz, "Real-time ultrasound imaging of muscles," *Muscle Nerve: Official J. Amer. Assoc. Electrodiagnostic Med.*, vol. 11, no. 1, pp. 56–65, 1988.

[33] P. Hodges, L. Pengel, R. Herbert, and S. Gandevia, "Measurement of muscle contraction with ultrasound imaging," *Muscle Nerve: Official J. Amer. Assoc. Electrodiagnostic Med.*, vol. 27, no. 6, pp. 682–692, 2003.

[34] C. Castellini, G. Passig, and E. Zarka, "Using ultrasound images of the forearm to predict finger positions," *IEEE Trans. Neural Syst. Rehabil. Eng.*, vol. 20, no. 6, pp. 788–797, Nov. 2012.

[35] N. Akhlaghi et al., "Real-time classification of hand motions using ultrasound imaging of forearm muscles," *IEEE Trans. Biomed. Eng.*, vol. 63, no. 8, pp. 1687–1698, Aug. 2016.

[36] S. Sikdar et al., "Novel method for predicting dexterous individual finger movements by imaging muscle activity using a wearable ultrasonic system," *IEEE Trans. Neural Syst. Rehabil. Eng.*, vol. 22, no. 1, pp. 69–76, Jan. 2014.

[37] Z. Sheng, N. Sharma, and K. Kim, "Quantitative assessment of changes in muscle contractility due to fatigue during NMES: An ultrasound imaging approach," *IEEE Trans. Biomed. Eng.*, vol. 67, no. 3, pp. 832–841, Mar. 2020.

[38] Q. Zhang, K. Lambeth, Z. Sun, A. Dodson, X. Bao, and N. Sharma, "Evaluation of a fused sonomyography and electromyography-based control on a cable-driven ankle exoskeleton," *IEEE Trans. Robot.*, vol. 39, no. 3, pp. 2183–2202, Jun. 2023.

[39] Z. Sheng, N. Sharma, and K. Kim, "Ultra-high-frame-rate ultrasound monitoring of muscle contractility changes due to neuromuscular electrical stimulation," *Ann. Biomed. Eng.*, vol. 49, pp. 262–275, 2021.

[40] Z. Sun, X. Bao, Q. Zhang, K. Lambeth, and N. Sharma, "A tube-based model predictive control method for joint angle tracking with functional electrical stimulation and an electric motor assist," in *Proc. IEEE Amer. Control Conf.*, 2021, pp. 1390–1395.

[41] T. Englert, A. Völz, F. Mesmer, S. Rhein, and K. Graichen, "A software framework for embedded nonlinear model predictive control using a gradient-based augmented lagrangian approach (GRAMPC)," *Optim. Eng.*, vol. 20, pp. 769–809, 2019.

[42] A. Savitzky and M. J. Golay, "Smoothing and differentiation of data by simplified least squares procedures," *Anal. Chem.*, vol. 36, no. 8, pp. 1627–1639, 1964.

[43] Z. Sheng, A. Iyer, Z. Sun, K. Kim, and N. Sharma, "A hybrid knee exoskeleton using real-time ultrasound-based muscle fatigue assessment," *IEEE/ASME Trans. Mechatron.*, vol. 27, no. 4, pp. 1854–1862, Aug. 2022.

[44] V. Molazadeh, Q. Zhang, X. Bao, B. E. Dicianno, and N. Sharma, "Shared control of a powered exoskeleton and functional electrical stimulation using iterative learning," *Front. Robot. AI*, vol. 8, 2021, Art. no. 711388.

[45] B. Xian, D. M. Dawson, M. S. De Queiroz, and J. Chen, "A continuous asymptotic tracking control strategy for uncertain nonlinear systems," *IEEE Trans. Autom. Control*, vol. 49, no. 7, pp. 1206–1211, Jul. 2004.

[46] J. Chae, L. Sheffler, and J. Knutson, "Neuromuscular electrical stimulation for motor restoration in hemiplegia," *Topics Stroke Rehabil.*, vol. 15, no. 5, pp. 412–426, 2008.

[47] L. Griffin et al., "Functional electrical stimulation cycling improves body composition, metabolic and neural factors in persons with spinal cord injury," *J. Electromyogr. Kinesiol.*, vol. 19, no. 4, pp. 614–622, 2009.

Krysten Lambeth received the B.Sc. degree in mathematics from Salem College, Winston-Salem, NC, USA, in 2019. She is currently working toward the Ph.D. degree in biomedical engineering with the Joint Department of Biomedical Engineering, North Carolina State University, Raleigh, NC, USA, and The University of North Carolina at Chapel Hill, Chapel Hill, NC, USA.

Her research interests include model predictive control, data-driven modeling, and bio-inspired control of rehabilitation robotics.

Mayank Singh received the B.Tech. degree in electrical & electronics engineering from Delhi Technological University, New Delhi, India, in 2018. He is currently working toward the Ph.D. degree in electrical engineering with NC State University, Raleigh, NC, USA.

He is interested in advancing rehabilitation assistive devices for mobility in impaired individuals. His research focuses on developing reinforcement learning and MPC based data-driven control methods for lower limb rehabilitation.

Christine Cleveland received the M.D. degree from the University of North Carolina at Chapel Hill, Chapel Hill, North Carolina, USA, in 2009.

She is currently an Assistant Professor of physical medicine & rehabilitation with the University of North Carolina (UNC) at Chapel Hill, NC, USA. She completed a Spinal Cord Injury fellowship with the University of Pittsburgh, Pittsburgh, PA, USA, in 2014. Most recently, she worked as a Clinical Assistant Professor with the University of Pittsburgh-School of Medicine. She practices at UNC's Memorial Hospital and the UNC Center for Rehabilitation Care.

Ashwin Iyer received the B.S. degree in mechanical engineering and a minor in computer science from University of Pittsburgh, Pittsburgh, PA, USA, in 2017, and the Ph.D. degree in biomedical engineering focusing on control methods using ultrasound imaging, North Carolina State University, in 2023.

He is currently working with Delsys, Inc, MA, USA.

Ziyue Sun received the B.Sc. and M.Sc. degree in mechanical engineering from University of Pittsburgh, Pittsburgh, PA, USA, in 2014 and 2017, respectively, and the Ph.D. degree in biomedical engineering from the University of North Carolina at Chapel Hill (UNC), Chapel Hill, NC, USA and North Carolina State University (NCSU), Raleigh, NC, USA, in 2022.

He is currently working with Didi Labs, Mountain View, CA, USA developing cutting-edge algorithms for the autonomous vehicle.

Nitin Sharma received the Ph.D. degree in mechanical engineering from the University of Florida, Gainesville, Florida, USA, in 2010.

He is currently an Associate Professor with the Joint Department of Biomedical Engineering, North Carolina State University- Raleigh and University of North Carolina-Chapel Hill. His research in hybrid exoskeletons and Tremor suppression is funded by NSF awards and NIH.

Prof. Sharma was a recipient of the NSF CAREER Award in 2018, IEEE Control Systems Technology Award 2019, and NIBIB Trailblazer Award in 2021.